Large area multiturn superfluid phase slip gyroscope

Niels Bruckner[a] and Richard Packard
Department of Physics, University of California, Berkeley, California 94720

(Received 26 April 2002; accepted 15 November 2002)

We have built and tested a large area multiturn superfluid ^{4}He phase slip gyroscope. This device demonstrates quantum-mechanical phase coherence of superfluid ^{4}He over a macroscopic length scale (1.4 m). The sensing loop area of this device is two orders of magnitude larger than our proof-of-principle model, with an improvement in sensitivity of ~20 over any other superfluid ^{4}He gyroscope. We find that this rotation sensor has excellent long-term stability. In addition, there are no new noise sources preventing further enhancements in sensitivity. © *2003 American Institute of Physics.* [DOI: 10.1063/1.1536727]

I. INTRODUCTION

Sensitive gyroscopes have found many applications, ranging from inertial navigation[1] to such fundamental disciplines as geodesy[2] and general relativity.[3] Geophysicists are interested in rotation sensors that can be used to study seismic effects as well as lunar and solar tides. The magnitude of these geodetic effects (generally in the sub-mHz to μHz frequency range) are on the order of $\sim 10^{-8}\ \Omega_E$ where Ω_E is the Earth's rotation rate (72.9×10^{-6} rad/s). General relativity predicts that a rotating body (such as the Earth) will drag the local inertial frame (such as that defined by the axis of a gyroscope). For a gyroscope hovering above the Earth, this general relativistic effect is on the order of $\sim 10^{-10}\ \Omega_E$.

Among the current state of the art gyroscopes are those based on spinning balls,[3] ring lasers,[1] and interfering matter waves.[4–6] Despite the fact that spinning ball gyros are being used in Gravity Probe B to measure general relativistic effects,[3] spinning balls experience residual torques in the presence of gravity (e.g., for imperfect roundness) that make them a less than ideal candidate for Earth-based measurements.

On the other hand, ring lasers and matter-wave interferometers, which fall into a category of gyroscopes based on the Sagnac effect, are not subject to these gravitational torques. The Sagnac effect predicts that a phase shift, $\delta\phi$, will develop when a beam of particles propagates through an interferometer of area $\mathbf{A}$ rotating at the angular velocity $\mathbf{\Omega}$. This phase shift can be expressed as[7]

$$\delta\phi = \frac{4\pi\mathbf{\Omega}\cdot\mathbf{A}}{\lambda v}, \tag{1}$$

where λ and v are the wavelength and velocity of the particles, respectively. For particles of mass m, λ is the de Broglie wavelength given by $\lambda_{\mathrm{dB}} = h/(mv)$ where h is Planck's constant. From Eq. (1), it is easy to show that the rotation-induced phase shift of an interferometer using massive particles can exceed a light-based interferometer by the factor of $mc^2/(hf)$ (c is the speed of light, and f its frequency). For instance, the phase shift for a single ^{4}He atom is a factor of ~10^9 greater than that of a photon in a HeNe laser. In general, however, ring laser gyroscopes compensate for this large disadvantage by means of well developed techniques to measure very small phase shifts. The best reported short-term sensitivities of Sagnac gyroscopes are $0.8\times 10^{-5}\ \Omega_E/\sqrt{Hz}$ for the atom-interferometer[4] and $1.8\times 10^{-5}\ \Omega_E/\sqrt{Hz}$ for the ring laser gyroscope.[1] However, the stability and, hence, long-term sensitivity is not nearly as good for either of these devices.

Here, we report on the development of a superfluid ^{4}He gyroscope which is essentially drift free and may, therefore, be ideally suited for sensitive longer-term measurements. We have increased the sensing area by almost 2 orders of magnitude over our previously reported efforts.[8,9] The subsequent gain in sensitivity now exceeds other published ^{4}He gyroscopes[10,11] by a factor of 20. In addition, we report on the excellent long-term stability of this type of device for frequencies measured down to ~10 μHz. We have found no new sources of noise that may prevent substantial enhancements in sensitivity.

II. SUPERFLUID ^{4}He INTERFEROMETER

For temperatures below 2.17 K, liquid ^{4}He exists as a superfluid[12] which can be described by a macroscopic quantum wave function of the form

$$\psi(\mathbf{r},t) = |\psi|\exp[\imath\phi(\mathbf{r},t)], \tag{2}$$

where $|\psi|$ and ϕ are, respectively, the amplitude and phase of this complex order parameter. A consequence of Eq. (2) is that the macroscopic superflow velocity, $\mathbf{v_s}$, is determined by the phase via the relation

$$\mathbf{v_s} = \frac{\hbar}{m_4}\nabla\phi, \tag{3}$$

where m_4 is the mass of a ^{4}He atom, and $\hbar$ is Planck's constant. Since the macroscopic wave function must be single valued, the circulation around any closed contour (in the inertial frame) is quantized according to

$$\oint \nabla\phi\cdot\mathbf{dl} = 2\pi n \Rightarrow \oint \mathbf{v_s}\cdot\mathbf{dl} = n\frac{h}{m_4} \equiv n\kappa_4$$

[a]Electronic mail: niels@physics.berkeley.edu

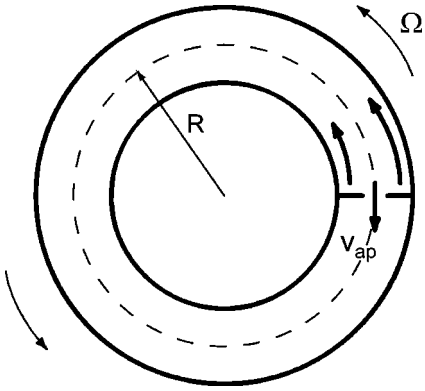

FIG. 1. Shown is a superfluid-filled torus, with average radius R, partitioned by a wall containing a small aperture. Rotation of the torus at angular velocity Ω induces backflow in the aperture given by Eq. (6).

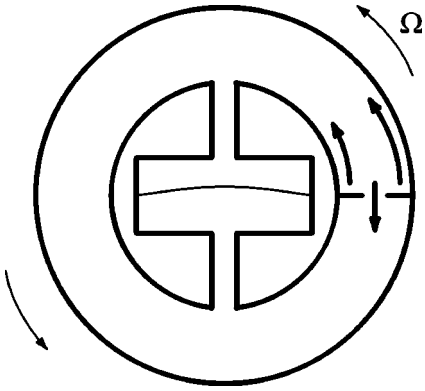

FIG. 2. The basic geometry of a diaphragm-aperture oscillator configured as a phase slip gyroscope. A soft flexible membrane (in the center of the figure) drives flow through the aperture and the toroidal path. The position of the membrane is monitored with a SQUID-based displacement sensor (not shown). The rotation-induced flow in the aperture shifts the apparent critical amplitude where phase slips occur.

$$n=0,\pm 1,\pm 2,\ldots, \tag{4}$$

where κ_4 is the quantum of circulation. The superfluid ^{4}He gyroscope is based on this quantization of circulation.[13]

We consider a superfluid-filled torus of radius R partitioned by a wall containing a small aperture (Fig. 1). If this torus is rotating slowly at an angular velocity $\mathbf{\Omega}$ then the moving wall will push the fluid in the torus arms at a velocity approximating solid body rotation ($v_s \simeq \Omega R$). At the same time, the superfluid will remain in its ground state with zero circulation ($n=0$). Evaluating the circulation (i.e., the line integral of the velocity) for a closed path that threads the aperture and the arms of the torus yields

$$\oint \mathbf{v_s}\cdot\mathbf{dl}=\int_{\text{arms}} \mathbf{v_s}\cdot\mathbf{dl}+\int_{\text{ap}} \mathbf{v_s}\cdot\mathbf{dl}=\Omega R\cdot 2\pi R+v_{\text{ap}}\cdot l_{\text{ap}}=0, \tag{5}$$

where v_{ap} and l_{ap} are, respectively, the velocity in and effective length of, the aperture. Therefore, rotation induces a backflow in the aperture with a value

$$v_{\text{ap}}=-\frac{2\pi R}{l_{\text{ap}}}\Omega R=-\frac{2\mathbf{\Omega}\cdot\mathbf{A}}{l_{\text{ap}}}, \tag{6}$$

where $\mathbf{A}$ is the area spanned by the arms of the torus. By expressing the velocity in the aperture in terms of the phase difference across the aperture [using Eq. (3)], it is straightforward to show that Eq. (6) is a restatement of the Sagnac phase shift in Eq. (1). The scalar product $\mathbf{\Omega}\cdot\mathbf{A}$ is known as the rotational flux and accounts for the general case when the normal vector of the area of the torus is not parallel to the rotation vector. For a multiturn torus with N loops, each with an area of A_0, we may make the substitution $A\rightarrow NA_0$. From Eq. (6), it is clear that if the circumference of the torus is macroscopic (e.g., $2\pi R\sim 1$ m) and the aperture is microscopic ($l_{\text{ap}}\sim 10^{-7}$ m), then this device behaves as a rotational velocity amplifier with a gain of $\sim 10^7$. The superfluid ^{4}He gyroscope is designed to measure this large rotationally induced velocity.

The technique used to measure the velocity in the aperture relies on the notion of a quantum phase slip, a concept introduced by Anderson[14] to explain how a superfluid can dissipate energy. Superflow through a small aperture remains dissipation free for velocities below a well defined critical velocity v_c, whose value is fixed for a given aperture and set of experimental conditions (i.e., temperature and pressure). When the flow velocity reaches v_c, a quantized vortex line[15] is nucleated and traverses the aperture. In crossing all the streamlines, the vortex grows in size and removes a discrete amount of energy from the flow. This process, whereby the phase difference across the aperture decreases by 2π (the velocity in the aperture decreases by $\Delta v_{\text{slip}}=\kappa_4/l_{\text{ap}}$) is known as a 2π phase slip.

The phase slip process and the critical velocity have been studied in detail in several laboratories.[16–19] The critical velocity is found to decrease linearly with temperature T; namely, $v_c=v_{c0}(1-T/T_0)$, where v_{c0} is the critical velocity extrapolated to zero temperature and $T_0\sim 2.5$ K. This linear temperature dependence can be deduced by assuming that the nucleation of phase slips relies on a thermal activation process. Furthermore, the stochastic nature of this thermal activation process implies that the critical velocity has a finite statistical width,[20] Δv_c, which will limit the precision of measuring v_c. We use these phase slips and the critical velocity to ascertain the rotation-induced flow in the aperture.

III. EXPERIMENTAL TECHNIQUE

The phase slip superfluid gyroscope uses a low-frequency diaphragm-aperture oscillator, similar to the device used to study individual phase slips.[21] The oscillator consists of a fluid pump with a soft flexible membrane coupled to the aforementioned torus (shown schematically in Fig. 2).

Electrostatic deflection of the soft membrane is used to push the superfluid through the small aperture and the parallel sensing loop. The position of the membrane is monitored with a superconducting quantum interference device (SQUID) based displacement transducer[22] capable of resolving $\sim 5\times 10^{-15}$ m/$\sqrt{\text{Hz}}$.

We drive the membrane with a sinusoidal force at the resonance frequency of the oscillator (typically, 10s of Hz). The flow through the aperture is comprised of three compo-

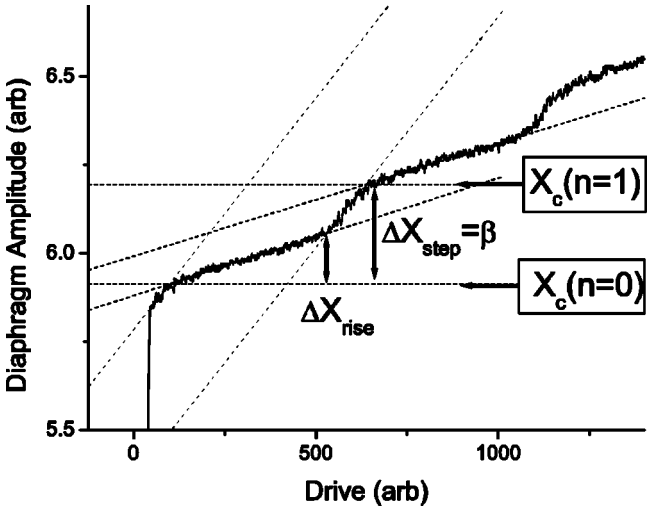

FIG. 3. This shows a staircase response for a real device (see Ref. 9). The slope of the step is proportional to Δv_c.

nents. The first component is the oscillating flow from the driven membrane. The amplitude of the membrane is directly proportional to the velocity of this oscillating flow. The second component is the rotation induced flow given by Eq. 6. The final component is flow produced by any configuration of trapped quantized vortex lines that might exist in the arms of the torus.

Phase slips occur when the total flow through the aperture reaches v_c. The critical oscillation amplitude of the membrane, X_c, is defined as the displacement amplitude of the membrane when the velocity in the aperture reaches v_c. If the rotation-induced flow increases by an amount $+\delta v_s$, then phase slips will occur for a critical oscillation amplitude lowered by the amount δX_c where $\delta X_c \propto -\delta v_s$. Our ability to extract the rotation-induced flow by monitoring this apparent critical amplitude presupposes that any flow produced by vortex lines remains constant. Indeed, we find this to be the case; therefore, for simplicity, we will assume that this vortex-induced flow is zero for the remainder of this article.

In practice, there are two different methods used to measure the rotation-induced flow: the staircase method and the slip-by-slip method.

A. Staircase method

The staircase technique is directly analogous to a method used to operate an rf SQUID. A plot of the peak amplitude of the membrane as a function of increasing electrostatic drive, results in a characteristic steplike pattern (Fig. 3). When the superfluid velocity in the aperture reaches v_c, the peak diaphragm amplitude saturates at a critical level given by[9]

$$X_c = \alpha v_c + \beta\left(n \mp \left|\frac{2\mathbf{\Omega}\cdot\mathbf{A}}{\kappa_4}\right|\right) \quad n = 0,1,2,\ldots, \tag{7}$$

where α and β are constants determined by the geometry of the oscillator. The choice of sign preceding the rotational flux in Eq. (7) depends on exactly where on the plateau the oscillator is being driven. The first half of the plateau is lowered ($-$ sign) and the second half is raised ($+$ sign) when rotational flux is added.[23]

The plateaus result from the fact that most of the energy being supplied to the oscillator is dissipated in the phase slip process. We consider the case of a staircase where the rotational flux is zero. Near the beginning of the first step, the probability of having a phase slip in a given half cycle of oscillation is near zero. At the middle of the step, this same probability reaches unity so that there is a slip every half cycle. By the end of the first step, there are two slips per half cycle. At this stage, the power supplied to the oscillator goes into increasing the amplitude until the power is large enough to produce additional slips, resulting in the formation of the second plateau.

In practice, the oscillator response is monitored at a fixed drive level. As shown by Eq. (7), rotation of the torus will shift the apparent critical amplitude. In addition, because of the scalar product in the rotation flux, reorienting the torus with respect to the rotation vector will also cause a change in the critical amplitude.

If the onset of v_c were a sharp deterministic transition, then the steps of the staircase would be horizontal. In reality, the finite width of Δv_c causes the steps to have a nonzero slope.[9] A measure of the quality of the staircase is given by the ratio of the step rise ΔX_{rise} to step height ΔX_{step}, namely:

$$\eta \equiv \frac{\Delta X_{\text{rise}}}{\Delta X_{\text{step}}}. \tag{8}$$

From Fig. 3, it is clear that a well defined staircase should have $\eta < 1$. A more detailed analysis[24] reveals that η can be written as

$$\eta = 2\left(\frac{1+\mathsf{R}}{\mathsf{R}}\right)\frac{\Delta v_c}{\Delta v_{\text{slip}}} = 2\left(\frac{1+\mathsf{R}}{\mathsf{R}}\right)\left(\frac{\Delta v_c}{v_{c0}}\right)\left(\frac{v_{c0}}{\Delta v_{\text{slip}}}\right), \tag{9}$$

where

$$\mathsf{R} = \frac{\rho a_{\parallel}/l_{\parallel}}{\rho_s a_{\text{ap}}/l_{\text{ap}}}. \tag{10}$$

Here, l and a are the length and cross sectional areas of the parallel path (subscript $\parallel$) and the aperture (subscript ap), and ρ, ρ_s are the density and superfluid density, respectively. R is the ratio of the kinetic inductances of the two paths. The physical interpretation of R is that the current through the parallel path is R times as large as the current going through the small aperture.

One can get a feel for the quality of the staircase for typical experimental values of the parameters. Since R is a geometric property based on the dimensions of the parallel path and the aperture, we have good control over its value. Experimentally, one typically finds that $\Delta v_c/v_{c0} \sim 0.01 - 0.02$. On the other hand, the quantity $v_{c0}/\Delta v_{\text{slip}}$, also known as the zero temperature critical phase difference (in units of 2π) varies unpredictably from one aperture to the next. Although we have had apertures with $v_{c0}/\Delta v_{\text{slip}}$ as low as ~ 16, more typically, we find values near 40–60 and sometimes over 100. It is expected that smaller apertures (with larger slip velocities, $\Delta v_{\text{slip}} = \kappa_4/l_{\text{ap}}$) will produce lower critical phase differences. In practice, however, we have not observed this for apertures with effective lengths (which scale as $\sim\sqrt{a_{\text{ap}}}$) ranging from several microns down

to a few hundred nanometers. This may be due to the fact that the critical velocity is determined by surface structure on the scale of a few nanometers, something over which we do not have good experimental control at the present time.

For typical experimental values of $\Delta v_c/v_{c0}\sim 0.02$, and $\mathrm{R}\sim 10$, one would need to have an aperture with $v_{c0}/\Delta v_{\mathrm{slip}}\leqslant 23$ in order for a staircase to be resolvable (i.e., $\eta\simeq 1$). Since most of our present apertures have a critical phase difference over twice as large, the staircase patterns are washed out. When this is the case, one can resort to a different method of analysis.

B. Slip-by-slip method

Without a staircase, one can still measure the rotation-induced flow by tracking the circulation state as it changes with every single slip. Here we outline this procedure developed by the Saclay group.[25]

When there is a rotation-induced flow through the aperture, the apparent critical velocity will shift depending on the direction of the flow. The difference in the apparent critical velocity in the two directions (positive and negative) is directly proportional to this rotation-induced flow. More explicitly, the rotation-induced flux is

$$\frac{2\mathbf{\Omega}\cdot\mathbf{A}}{\kappa_4}=(|\Delta\phi^+|-|\Delta\phi^-|)\frac{1+\mathrm{R}}{(2\pi)\cdot 2\mathrm{R}}, \tag{11}$$

where we have used the more convenient notation of the phase difference, $\Delta\phi$, in lieu of the velocity through the aperture (the superscripts $+$ and $-$ refer to the two different directions of flow). The phase difference across the aperture is proportional to the velocity through the aperture and is given by

$$\frac{\Delta\phi}{2\pi}\equiv\frac{v_{\mathrm{ap}}}{\Delta v_{\mathrm{slip}}}. \tag{12}$$

The apparent phase difference for the two directions is directly related to the peak diaphragm amplitude X measured a quarter cycle earlier by

$$\frac{\Delta\phi^{\pm}}{2\pi}=\frac{\frac{\mp|X|}{\Delta X_{\mathrm{slip}}}+nR}{1+\mathrm{R}}, \tag{13}$$

where ΔX_{slip} is the decrease in diaphragm amplitude for a 2π phase slip, and n is the integer describing the circulation state of the loop.

The derivation of Eqs. (11) and (13) involves some algebra and is not reproduced here (see Ref. 24). This derivation is similar to that of Eq. (7), except that we are explicitly taking into account that both $\Delta\phi$ and X are signed quantities.

The raw data used in conjunction with Eq. (13) is obtained in the following manner. Experimentally, the oscillator is driven with a constant amplitude sinusoidal force at its resonance frequency. The full sinusoidal wave form of the oscillator is recorded and a parabola is fit near the extrema to determine the peak amplitude of each half cycle. We, therefore, collect a sequence of (signed) peak amplitudes X in arbitrary computer units. We plot the magnitude of the peak amplitude $|X|$ as a function of time (or half-cycle number).

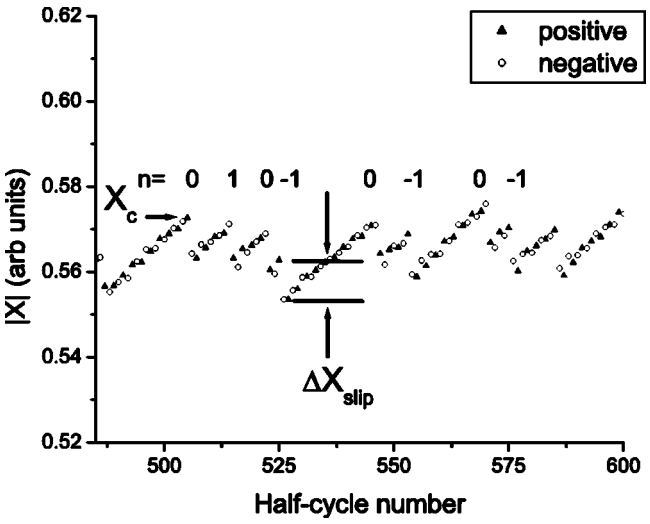

FIG. 4. The magnitude of the peak amplitude of the diaphragm $|X|$, is plotted for consecutive half cycles (both positive and negative displacements of the membrane). We record the critical amplitude, X_c, and the circulation state n for each phase slip in order to calculate the rotational flux. Data are from the 95 cm^2. The displacement amplitude for a phase slip, ΔX_{slip}, is approximately 10 pm.

Figure 4 shows a sample of such data for the present device (for similar data from the Saclay group, see Ref. 16). The smooth ramps are interrupted by sharp drops, which are identified as single phase slips. Each time a slip occurs, the circulation state changes by a single unit ($n\rightarrow n\pm 1$), where the sign is chosen such that the velocity in the aperture (or phase difference across it) always decreases.

Therefore, for each phase slip, we record n and X_c (i.e., the value of X when a phase slip occurs). We evaluate the phase difference corresponding to these quantities using Eq. (13). The rotation flux, in units of κ_4, is subsequently found by inserting these apparent phase differences (for the two directions of flow) into Eq. (11).

C. Noise

The precision with which we can measure rotational changes depends on the precision with which we can measure the phase slip critical velocity. Therefore, the fundamental limitation in the phase slip gyroscope sensitivity is the stochastic width of the critical velocity. The statistical uncertainty in the critical velocity σ_{v_c} (i.e., the standard deviation) leads to an uncertainty in the measurement of the peak displacement of the diaphragm, σ_{X_c}. Using Eq. (7), this uncertainty is simply $\sigma_{X_c}=\alpha\sigma_{v_c}$. The uncertainty in the rotation Ω after time τ is

$$\sigma_\Omega(\tau)=\frac{\partial\Omega}{\partial X_c}\sigma_{X_c}(\tau)=\left(\frac{\kappa_4}{2A}\right)\left(\frac{\alpha}{\beta}\right)\frac{\sigma_{v_c}}{\sqrt{\nu_{\mathrm{slips}}\tau}}, \tag{14}$$

where ν_{slips} is the average slip frequency such that N slips are measured in time τ (i.e., $N=\nu_{\mathrm{slips}}\tau$). If the phase slips are uncorrelated, one can introduce a white power spectral density S_Ω such that $\sigma_\Omega(\tau)=S_\Omega^{1/2}/\sqrt{\tau}$. Using the geometric formulas for α and β, the rotational noise spectral power density is

$$S_{\Omega}^{1/2}\left(\frac{\text{rad}}{\text{s}\sqrt{\text{Hz}}}\right)=\frac{1+\mathsf{R}}{\mathsf{R}}\frac{\Delta v_c}{\Delta v_{\text{slip}}}\left(\frac{\kappa_4}{2A}\right)\frac{1}{\sqrt{2\pi\nu_{\text{slips}}}}, \tag{15}$$

where we have used $\sigma_{v_c}=\Delta v_c/\sqrt{2\pi}$ for a Gaussian distribution. Therefore, for a given torus area A, the recipe for lowering the noise is to minimize $\Delta v_c/\Delta v_{\text{slip}}$, to maximize ν_{slips}, and to make $\mathsf{R}\gg 1$.

When dealing with staircases, it is more convenient to express the rotational noise in terms of the staircase parameter η. Using Eq. (9), the rotational noise is

$$S_{\Omega}^{1/2}\left(\frac{\text{rad}}{\text{s}\sqrt{\text{Hz}}}\right)=\frac{\eta}{2}\left(\frac{\kappa_4}{2A}\right)\frac{1}{\sqrt{2\pi\nu_{\text{slips}}}}. \tag{16}$$

The shape of the staircase, therefore, can be used to calculate the rotational noise of the device.

Two phase slip gyroscope prototypes have previously been reported. The Saclay group built a 4.0 cm^2 gyroscope and used the slip-by-slip method of analysis[10] because v_c for their aperture was too large to produce a staircase. Our group in Berkeley built a 1 cm^2 device and used the staircase method for analysis.[8] Consistent with the noise calculations just given, both devices showed rotational sensitivities of $\sim\Omega_E/\sqrt{\text{Hz}}$, where Ω_E is the Earth's rotation rate. Since those initial efforts, we have built several generations of larger devices, culminating with a large area multiturn gyroscope described below.

IV. LARGE AREA MULTITURN GYROSCOPE

Our most recent attempts to acquire an aperture with a low critical phase difference were unsuccessful. Since the staircase method requires a low critical phase difference, we built a device that could be operated with the slip-by-slip analysis. Two such gyroscopes were built: The first with a 10.6 cm^2 sensing loop and the second with a 95 cm^2 loop. This work focuses on the more sensitive 95 cm^2 device.

The multiturn 95 cm^2 is shown in Fig. 5. The sensing area consists of a helical path (with a total of 13 turns) wound on the front and back side of a thin square brass plate (4 cm wide and 2.5 mm thick). The nominal area of the loop is found by assuming that the position of the parallel channel is at the midpoint of the channel. The toroidal length is 1.41 m, and the channels are 0.78 mm wide and 0.25 mm deep. The aperture (0.42 μm$\times$0.26 μm) is etched in a 100 nm thick SiN membrane residing on a 3 mm Si chip[26] which is glued in the center of the central depression. The resulting R ratio for this geometry is 0.43. Rigid square plastic washers, glued to the raised surface on both the front and back sides, seal the channels.

A 7 μm thick metallized Kapton membrane, glued over the central depression (recessed 0.25 mm), acts as the pump that we use to push fluid through the aperture and parallel path. Starting from the central depression, fluid moves through the parallel path and the aperture. The fluid moving through the parallel path winds through the arms on the front side, goes through a large hole to the back side of the plate, and continues its path through the back side channels until it reaches the back side of the aperture.

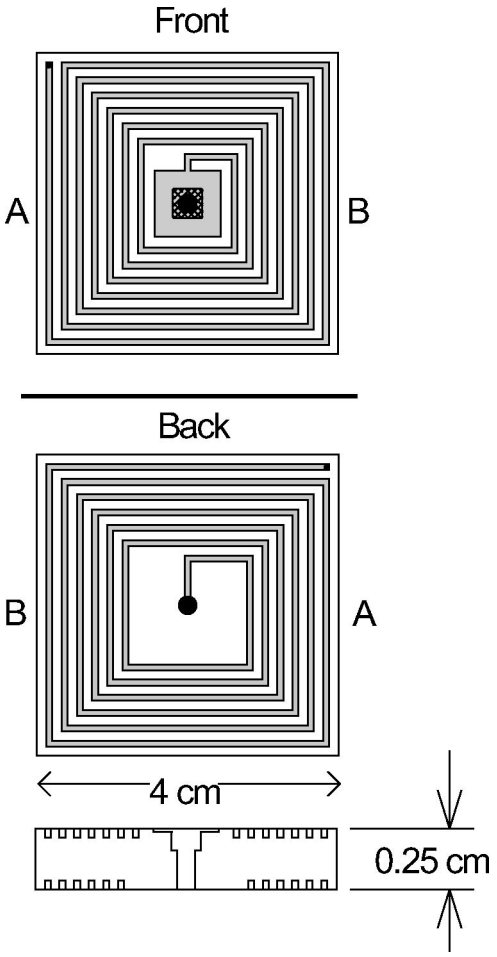

FIG. 5. A sketch of the front and back views of the multiturn 95 cm^2 gyroscope with a well defined flow path. The aperture is glued into the inner central depression. The sensing loop, machined in brass, winds around clockwise on the front, continues through a large drilled hole to the back side, and continues looping around in the same direction (counterclockwise from the back side point of view), until it reaches the back side of the aperture. The front side is sealed with a 7 μm Kapton membrane and a stiff 0.125 mm plastic washer to insure the rigidity of the flow channels. The back side channels are sealed with a single 0.125 mm plastic washer with a central through hole to allow the fluid to move in and out. The depth of the various features: (white) raised surface, (gray) recess 0.25 mm, (crosshatch) recess 0.9 mm, and (black) through hole.

This plate is immersed in a superfluid-filled box which is cooled with an adsorption pumped ^{3}He refrigerator. At our base operating temperature of 0.28 K, the oscillator has a resonance frequency of 7.073 Hz and a quality factor $\sim$20 000.

To determine the sensitivity of the gyroscope, we measure the change in the rotation-induced flow as the sensing loop area is reoriented with respect to the local component of the Earth's rotation vector (see Fig. 6). In the lab, the normal to the sensing loop area is in the horizontal plane. The gyroscope is rigidly fixed to the refrigerator which can run at a temperature near 0.30 K for $\sim$36 h at a time. The refrigerator is placed inside a helium dewar which resides on a rotating platform consisting of two flat centered aluminum disks separated by a water bearing. A dc motor coupled by a pulley system is used to reorient the dewar/gyroscope system.

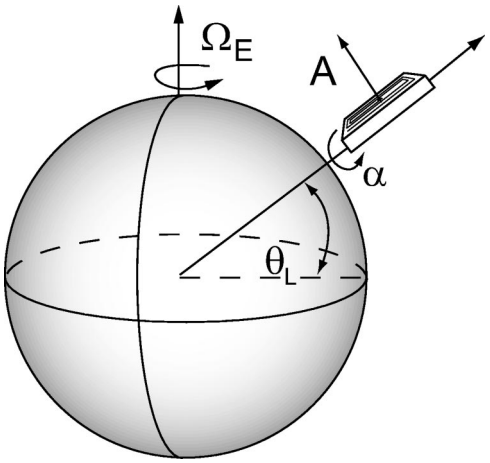

FIG. 6. The magnitude of the Earth's rotational flux is varied by reorienting the gyroscope sensing area **A** (where **A** is normal to the plane of the loop) with respect to the Earth's rotation vector, $\mathbf{\Omega_E}$. This is done by reorienting the gyroscope about the vertical axis in the lab. At a latitude θ_L, the rotational flux varies with orientation angle α as $2\Omega_E A \cos\theta_L \cos\alpha$.

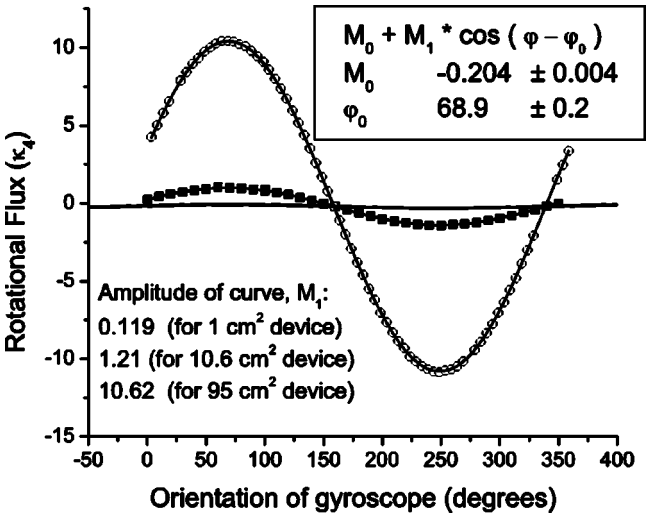

FIG. 7. Shown is the Earth's rotational flux as a function of the orientation of the sensing loop area of the gyroscope. The present 95 cm^2 device is compared with two previous ^{4}He gyroscopes that have been built in Berkeley: the prototype 1 cm^2 gyroscope (see Ref. 8) (whose modulation curve on this scale looks like a flat line), and a 10.6 cm^2 device. M_0 is a dc offset determined by the flow induced by remnant vortices.

As seen in Eq. (6), when we reorient the gyroscope about the vertical axis in the lab, the rotational flux is expected to vary as $2\Omega_E^{\mathrm{Berk}} A \cos\alpha$ where Ω_E^{Berk} is the projection of the Earth's rotation at our latitude ($\theta_L = 37\mathrm{N}\ 52'\ 20''$) in Berkeley (i.e., $\Omega_E^{\mathrm{Berk}} = \Omega_E \cos\theta_L$) and α is the angle between **A** and $\mathbf{\Omega_E^{Berk}}$. Without prior knowledge of the direction of true North, we measure the rotational flux with respect to some convenient lab coordinate system, characterized by an angle which is offset from α.

At a fixed orientation, we find the rotational flux by recording the half-cycle peak amplitude for a period of 10 min, as described in Sec. III B. A typical 10 min data record contains ~2800 slips for analysis which would allow us to resolve the rotational flux to $\sim 0.01\kappa_4$. After this measurement, the dewar is reoriented slowly by 5° at a rate of ~2°/min. We allow the system to settle for ~5 min at the new orientation angle before recording another 10 min of data. We repeat this process until the gyroscope has been reoriented by 360° which, for a measurement of 72 points separated by 5°, takes ~21 h.

A plot of the rotational flux versus orientation angle produces the predicted cosinusoidal response curve (also known as the modulation curve). A typical modulation curve for this device is shown in Fig. 7. We measure the amplitude of the modulation due to the Earth's rotational flux to be $2\Omega_E^{\mathrm{Berk}} A = (10.63 \pm 0.01)\kappa_4$, an agreement of better than 3% to that expected for a 95 cm^2 loop. We locate true North with a precision of ~0.4°, which represents the reproducibility of the offset angle from one modulation curve to the next (68.9° is the offset of the arbitrarily chosen dewar coordinate system from North, the direction where the rotational flux is at a maximum).

The sensitivity of this device to the Earth's rotational flux is highest at a region of maximum slope on the modulation curve. The long-term stability of this device was recorded by measuring the rotational flux at the point of maximum sensitivity for 30 h. In order to generate the rotational noise power spectrum, the 30 h time trace was divided into 3000 bins of 36 s each. For each bin, the rotational flux was found using the slip-by-slip analysis described in Sec. III B. In these 30 h runs, which must obviously be conducted during both day and night, occasionally external disturbances are large enough to render identifying individual slips impossible. In these instances, short segments of data are removed. The long-term stability of the circulation bias makes it possible to piece together these disjointed segments. The bin size of 36 s was chosen so that no one segment would have less than ~1/2 the average number of slips for the other segments (169.2 slips/bin). We estimate that ~1500 slip events are omitted from this 30 h measurement, compared to 507 689 total included slips (99.7%).

Figure 8 shows the change in the rotational flux (in units of the Earth's rotation rate) for this 30 h measurement, and Fig. 9 shows the corresponding rotational noise power spec-

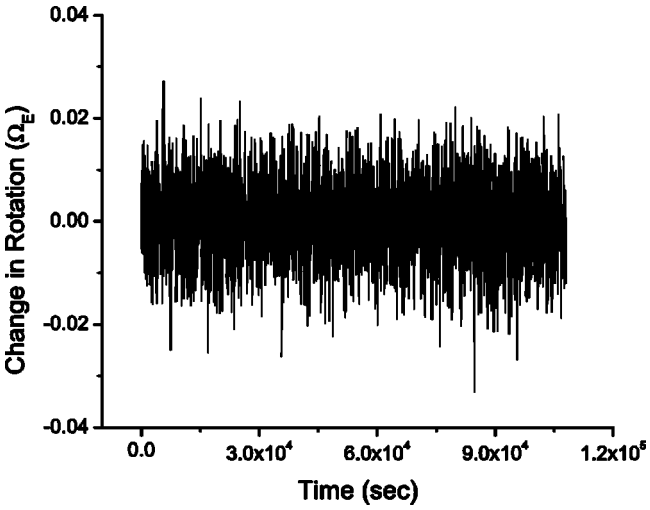

FIG. 8. Shown is the long-term stability of the 95 cm^2 device over a 30 h period. Each data point is a 36 s average.

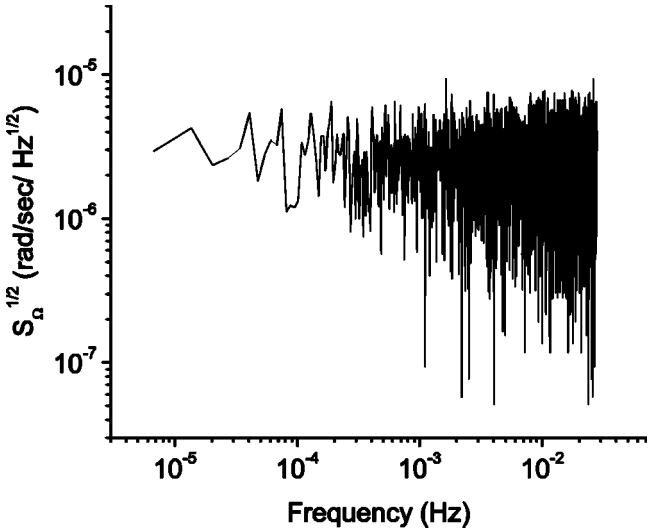

FIG. 9. Shown is the rotational noise spectrum for the 95 cm^2 device (the fast Fourier transform of Fig. 8). The mean value is 2.6 μrad/s/$\sqrt{\text{Hz}}$ which corresponds to $3.5\times10^{-2}\ \Omega_E/\sqrt{\text{Hz}}$.

trum. This power spectrum is ''white'' and has a mean value of 2.6 μrad/s/$\sqrt{\text{Hz}}$. Therefore, the useful sensitivity of this large area multiturn phase slip gyroscope is $3.5\times10^{-2}\ \Omega_E/\sqrt{\text{Hz}}$.

The most striking feature of these results is the absence of low-frequency noise in the rotational power spectrum. We believe that the device contains remnant vorticity due to the existence of a nonzero value of the circulation bias even when the gyroscope is oriented so that its rotational flux is zero. However, the stability of the circulation bias over this 30 h time scale indicates that the movement of remnant vortices is minimal when we do not disturb the system. In addition, we have not observed any bias shifts during any of the $\sim$15 modulation curve measurements recorded with this device or the previous 10.6 cm^2 device, even though we disturb the system every time we reorient the dewar.

In an attempt to quantify the level of disturbance needed to change the bias, we drop a computer mouse ball ($\sim$30 g) onto the dewar platform from various elevations. We find that the bias does not shift when the ball is dropped from a height of $\sim$1 cm, but the bias does change when we drop the ball from $\sim$10 cm. Apparently, the latter case is a more severe disturbance than one might encounter while reorienting the dewar, even for our highest possible reorientation rate of $\sim$20°/min.

Larger volume devices may have an increased susceptibility to external disturbances which in turn could move remnant vortices off their pinning sites. If this subsequently becomes a problem, it will be necessary to fill the device with a porous substance such as aerogel. However, we have not observed any adverse stability effects, even as the volume of this 95 cm^2 gyroscope has exceeded that of our prototype by $\sim$2 orders of magnitude.

V. PROSPECTS FOR IMPROVED SENSITIVITY

Using Eqs. (9) and (16), the rotational resolution of the phase slip gyroscope can be written as

$$S_\Omega^{1/2}\left(\frac{\text{rad}}{\text{s}\sqrt{\text{Hz}}}\right)=\frac{1+\mathsf{R}}{\mathsf{R}}\left(\frac{\Delta v_c}{v_{c0}}\right)\left(\frac{v_{c0}}{\Delta v_{\text{slip}}}\right)\left(\frac{\kappa_4}{2A}\right)\frac{1}{\sqrt{2\pi\nu_{\text{slips}}}}. \tag{17}$$

Gains in sensitivity will come primarily from increases in the area of the loop and the operating frequency of the oscillator.

One can imagine building an even more sensitive gyroscope with the following parameters: 15 turns of a 1 m diameter loop; a channel radius of 3 mm; a circular aperture with a 50 nm radius in a 50 nm thick substrate; a 9 cm^2 diaphragm with a spring constant of $\sim$1500 N/m; $\mathsf{R}=10$; $\Delta v_c/v_{c0}=0.01$; and a zero-temperature critical phase difference ($v_{c0}/\Delta v_{\text{slip}}$) of 15. The resonance frequency of such a diaphragm-aperture oscillator would be $\sim$0.5 Hz and its sensitivity, if Eq. (17) continues to hold, would be $\sim5\times10^{-6}\ \Omega_E/\sqrt{\text{Hz}}$.

In order to operate at a higher frequency, one would need to find a mode other than the fundamental diaphragm-aperture resonance that can be used to generate phase slips in the aperture. The derivation of the resonance frequency of the diaphragm-aperture oscillator assumes that the superfluid is incompressible. This assumption is no longer valid if we, for instance, stiffen the diaphragm in order to increase the fundamental resonance of the diaphragm-aperture above $c/l_\parallel$ where c is the speed of sound (240 m/s) and $l_\parallel$ is the length of the toroidal path. For the gyroscope just described, with $l_\parallel\sim47$ m, this implies that the diaphragm-aperture resonance frequency needs to be $\ll5$ Hz.

However, one could operate the gyroscope at higher frequencies by utilizing the acoustical modes that exist in the sensing loop. Simulations have been performed[27] to address this possibility. The results suggest that using higher harmonics of these acoustical modes introduces additional noise that actually degrades the sensitivity in most, but not all, cases. This noise arises from sound waves generated by phase slips in previous half cycles. Using the lowest harmonic for a 1 m diameter loop, where $\nu\sim80$ Hz, $\mathsf{R}=10$, and $\Delta v_c/\Delta v_{\text{slip}}\simeq0.1$, the authors of Ref. 27 find the sensitivity to be $\sim2\times10^{-9}$ rad/s/$\sqrt{\text{Hz}}$ (or $3\times10^{-5}\ \Omega_E/\sqrt{\text{Hz}}$), an order of magnitude worse than that predicted by Eq. (17). The possibility that the coupling of this additional noise can be reduced by careful design of the hydrodynamical circuit remains an open question. In addition, it may be possible to damp the sound modes with an absorbing material such as aerogel. Further experimentation is needed to address these issues.

However, from a practical standpoint, one needs a method for testing these gyroscopes when the random environmental rotational signals exceed the intrinsic sensitivity of the device. Velocity sensors attached to the cell stage reveal that in quiet conditions (i.e., vibration and acoustic isolation mechanisms fully operational) the velocity of the low-temperature stage at a typical pendulum mode frequency of $\sim$15 Hz often exceeds $\sim$100 nm/s. This corresponds to a peak-to-peak motion of at least several nanometers. If this oscillation is produced by a pendulum with a length of $\sim$10 cm, then the rotational velocity already exceeds 1 μrad/s, or $\sim10^{-2}\ \Omega_E$.

Here, we suggest two methods that allow us to characterize the intrinsic sensitivity of a gyroscope in the presence

of a noisy rotational environment. The first technique is to reduce the effective area of the sensing loop to zero by winding an astatic pickup loop where the toroidal path on the back of the plate is wound in a direction opposite to that of the front. Extrinsic noise sources (i.e., vortex motion and coupling to external disturbances) should be independent of the shape of the sensing loop. A lower noise level for the astatic loop device would confirm that external rotational noise signals exceed the intrinsic sensitivity. A second technique is to push the operating frequency of the gyroscope to frequencies much higher than the parasitic pendulum modes that produce the random rotational signals. In this scenario, the external rotational *noise* peaks are actually rotational *signals* which will show up as low-frequency lines modulating the rotation-induced flow. The sensitivity of the gyroscope is simply determined by the noise floor that results from subtracting these *signals*. The development of more sensitive large area gyroscopes will likely yield other useful techniques for measuring the intrinsic sensitivity in the presence of a noisy rotational environment.

VI. CONCLUSION

We have built a multiturn superfluid ^{4}He phase slip gyroscope which demonstrates a sensitivity of 2.6 μrad/s/$\sqrt{\text{Hz}}$ for frequencies down to ~ 10 μHz. The noise of this device is limited by the stochastic width of the phase slip process. We have found no evidence of other intrinsic limitations despite the fact that the scale of the gyroscope (sensing loop area and volume) have increased by 2 orders of magnitude.

Improvements in the sensitivity of the phase slip gyroscope will primarily come from increasing the sensing loop area as well as the operating frequency of the device. The main experimental question is whether it will be possible to utilize the higher frequency acoustic modes of the toroidal path in order to access these higher frequencies. We have discussed two techniques which can be used to measure the intrinsic sensitivity independent of the ambient rotational noise (which will likely exceed the intrinsic sensitivity of the gyroscope).

Although the sensitivity of the present device is still between $\sim 3-4$ orders of magnitude less than the short-term sensitivities of ring laser gyroscopes[1] and atom interferometers,[4] the long-term stability of the superfluid ^{4}He gyroscope could eventually make it an attractive option for geophysical applications, which have signals in the sub-mHz to μHz frequency range.

ACKNOWLEDGMENTS

The authors thank A. Amar, J. C. Davis, and K. Schwab for help with earlier versions of this experiment and K. Penanen for many useful conversations. One of the authors (R.P.) would like to thank Professor K. LaRana from Universita' di via Gabbiola for his seminal contributions to this work. This work was supported in part by the National Science Foundation and the National Aeronautics and Space Administration. Another author (N. B.) was supported by a NASA Graduate Student Research Fellowship.

[1] G. E. Stedman, Rep. Prog. Phys. **60**, 615 (1997).
[2] B. F. Chao, EOS, Amer. Geophys. Union **72**, 550 (1991).
[3] S. Buchman, C. W. F. Everitt, B. Parkinson, J. P. Turneaure, and G. M. Keiser, Physica B **280**, 497 (2000).
[4] T. L. Gustavson, A. Landragin, and M. A. Kasevich, Class. Quantum Grav. **17**, 2385 (2000).
[5] A. Lenef, T. D. Hammond, E. T. Smith, M. S. Chapman, R. A. Rubenstein, and D. E. Pritchard, Phys. Rev. Lett. **78**, 760 (1997).
[6] F. Riehle, T. Kisters, A. Witte, J. Helmcke, and C. J. Borde, Phys. Rev. Lett. **67**, 177 (1991).
[7] J. F. Clauser, Physica B **151**, 262 (1988).
[8] K. Schwab, N. Bruckner, and R. E. Packard, Nature (London) **386**, 585 (1997).
[9] K. Schwab, N. Bruckner, and R. Packard, J. Low Temp. Phys. **110**, 1043 (1998).
[10] O. Avenel and E. Varoquaux, Czech. J. Phys. **46**, 3319 (1996).
[11] O. Avenel, P. Hakonen, and E. Varoquaux, Phys. Rev. Lett. **78**, 3602 (1997).
[12] D. R. Tilley and J. Tilley, *Superfluidity and Superconductivity* (Wiley, New York, 1990).
[13] R. Packard and S. Vitale, Phys. Rev. B **46**, 3540 (1992).
[14] P. W. Anderson, Rev. Mod. Phys. **38**, 298 (1966).
[15] A vortex line is a filament that has stable currents concentric with the filament.
[16] E. Varoquaux, O. Avenel, and M. W. Meisel, Can. J. Phys. **65**, 1377 (1987).
[17] A. Amar, Y. Sasaki, R. Lozes, J. C. Davis, and R. E. Packard, Phys. Rev. Lett. **68**, 2624 (1992).
[18] G. M. Schifflett and G. B. Hess, J. Low Temp. Phys. **98**, 591 (1995).
[19] W. Zimmermann, Jr., Contemp. Phys. **37**, 219 (1996).
[20] For the definition of Δv_c, we follow the convention of E. Varoquaux, W. Zimmermann, Jr., and O. Avenel, in *Excitations in Two-dimensional and Three-Dimensional Quantum Fluids*, edited by A. F. Wyatt and H. J. Lauter (Plenum, New York, 1991). For a Gaussian distribution, this width is related to the standard deviation σ_{v_c} by $\sigma_{v_c}=\Delta v_c/\sqrt{2\pi}$.
[21] O. Avenel and E. Varoquaux, Phys. Rev. Lett. **55**, 2704 (1985).
[22] O. Avenel and E. Varoquaux, in *Proceedings of the XIth International Cyrogenic Engineering Conference*, edited by G. Klipping and I. Klipping (Butterworths, London, 1986), pp. 587–591.
[23] The largest physically distinguishable rotational flux is half a quantum of circulation. A plot of X_c versus Ω would result in a triangle pattern with periodicity of $\kappa_4/(2A)$.
[24] N. Bruckner, Ph.D. thesis, University of California at Berkeley, 2002.
[25] O. Avenel, P. Hakonen, and E. Varoquaux, J. Low Temp. Phys. **110**, 709 (1998).
[26] A. Amar, R. Lozes, Y. Sasaki, J. C. Davis, and R. E. Packard, J. Vac. Sci. Technol. B **11**, 259 (1993).
[27] Y. Mukharsky, O. Avenel, and E. Varoquaux, J. Low Temp. Phys. **113**, 915 (1998).